REPORT DOCUMENTATION PAGE

Form Approved
OMB No. 0704-0188

1. REPORT DATE *(DD-MM-YYYY)*	**2. REPORT TYPE**	**3. DATES COVERED** *(From - To)*
November 2012	Technical Paper	November 2012-January 2013

4. TITLE AND SUBTITLE
Analysis of Self-Excited Combustion Instabilities Using Decomposition Techniques

5a. CONTRACT NUMBER
In-House

5b. GRANT NUMBER

5c. PROGRAM ELEMENT NUMBER

6. AUTHOR(S)
Huang, C., Anderson, W., Harvazinski, M. and Sankaran, V.

5d. PROJECT NUMBER

5e. TASK NUMBER

5f. WORK UNIT NUMBER
5K-61RZS

7. PERFORMING ORGANIZATION NAME(S) AND ADDRESS(ES)

Air Force Research Laboratory (AFMC)
AFRL/RQR
5 Pollux Drive.
Edwards AFB CA 93524-7048

8. PERFORMING ORGANIZATION REPORT NO.

9. SPONSORING / MONITORING AGENCY NAME(S) AND ADDRESS(ES)
Air Force Research Laboratory (AFMC)
AFRL/RQR
5 Pollux Drive
Edwards AFB CA 93524-7048

10. SPONSOR/MONITOR'S ACRONYM(S)

11. SPONSOR/MONITOR'S REPORT NUMBER(S)
AFRL-RQ-ED-TP-2012-479

12. DISTRIBUTION / AVAILABILITY STATEMENT
Distribution A: Approved for Public Release; Distribution Unlimited. PA#13030

13. SUPPLEMENTARY NOTES
Conference paper for the 51st AIAA Aerospace Sciences Meeting, Grapevine, Texas, 7-10 January 2013.

14. ABSTRACT

Proper orthogonal decomposition (POD) and dynamic mode decomposition (DMD) are compared with traditional band-pass filtering based analysis for the study of self-excited combustion instabilities in a longitudinal mode rocket combustor. The POD analysis approximates the complex high-rank dynamics with simple lower-rank expressions for the mode shapes. Each POD mode, however, is comprised of multiple acoustic frequencies and specific modes of the pressure and heat release are not related, which makes the analysis more qualitative. On the other hand, the DMD analysis generates a global frequency spectrum and each mode corresponds to a specific discrete frequency. The DMD result therefore provide a quantitative means for understanding the relationship between the pressure modes and the heat release modes and for establishing the driving mechanisms responsible for the incidence of combustion instabilities. The paper uses these analyses to describe the Rayleigh index on a modal basis to shed light on the frequency-based response of the combustor flowfield.

15. SUBJECT TERMS

16. SECURITY CLASSIFICATION OF:			**17. LIMITATION OF ABSTRACT**	**18. NUMBER OF PAGES**	**19a. NAME OF RESPONSIBLE PERSON**
					Venkateswaran Sankaran
a. REPORT	**b. ABSTRACT**	**c. THIS PAGE**			**19b. TELEPHONE NO** *(include area code)*
Unclassified	**Unclassified**	**Unclassified**	SAR	19	661-525-5534

Standard Form 298 (Rev. 8-98)
Prescribed by ANSI Std. 239.18

Analysis of Self-Excited Combustion Instabilities Using Decomposition Techniques

Cheng Huang[1], William E. Anderson[2]
Purdue University, West Lafayette, IN, 47907

and

Matthew E. Harvazinski[3], Venkateswaran Sankaran[4]
Air Force Research Laboratory (AFRL), Edwards AFB, CA, 93524

Proper orthogonal decomposition (POD) and dynamic mode decomposition (DMD) are compared with traditional band-pass filtering based analysis for the study of self-excited combustion instabilities in a longitudinal mode rocket combustor. The POD analysis approximates the complex high-rank dynamics with simple lower-rank expressions for the mode shapes. Each POD mode, however, is comprised of multiple acoustic frequencies and specific modes of the pressure and heat release are not related, which makes the analysis more qualitative. On the other hand, the DMD analysis generates a global frequency spectrum and each mode corresponds to a specific discrete frequency. The DMD result therefore provide a quantitative means for understanding the relationship between the pressure modes and the heat release modes and for establishing the driving mechanisms responsible for the incidence of combustion instabilities. The paper uses these analyses to describe the Rayleigh index on a modal basis to shed light on the frequency-based response of the combustor flowfield.

I. Introduction

Data processing techniques based on proper orthogonal decomposition (POD) and dynamic model decomposition (DMD) are powerful and elegant methods which are used to obtain a low-dimensional approximate description of high-dimensional physical processes. POD has been extensively employed in the study of turbulence for cold flow due to the limitations of experimental measurements in terms of both temporal and spatial resolution.[1-3] POD can also be used to extract mode shapes and basis functions. Its application in combustion problems has received some attention recently, [4-6] where it has been used to gain insight into flame dynamics. DMD is a new technique that has not yet been extensively used for reacting flow analysis. Thus far most of DMD's applications have been investigations of flowfield characteristics.[7-9]

Traditional data processing in combustion instability analysis involves band-pass filtering of the data around the frequencies determined from a power spectral density (PSD) analysis of the raw signal. In this way, the correlation between acoustic and combustion can be explored within a certain frequency range. However, in many cases, filtered results are sensitive to the filtering methods. Moreover, information about the couplings between frequencies might be lost by band-passing the signals. One primary advantage of the decomposition techniques over filtering is that they deal with the whole data with minimum information loss. Moreover, unlike filtering techniques, POD and DMD do not require a prior knowledge or pre-analysis of the underlying physical and chemical phenomena. Another motivation is that they are capable of extracting dynamically significant structures from the flowfield of concern. [4-5] Each decomposed mode can be represented in terms of a spatial response and a temporal response, which can in turn provide detailed insight into the dynamics of acoustic and combustion.

[1] Graduate Research Assistant, School of Mechanical Engineering and Student Member AIAA.
[2] Professor, School of Aeronautics and Astronautics and Associate Fellow AIAA.
[3] Scientist, Rocket Propulsion Division and Member AIAA.
[4] Senior Scientist, Rocket Propulsion Division and Senior Member AIAA.

In this paper, our emphasis is on the exploratory applications of POD and DMD for self-excited combustion instability in a gas-gas coaxial rocket injector, the simulation of which was conducted by Harvzinski et al.[10, 11] Moreover, distorted triple flame has been found using large-eddy simulation of the same geometry by Garby et al.[12] Experimental measurements of this configuration have been published previously and recent results are given by Feldman et al.[13] The present POD and DMD analyses are carried out using the afore-mentioned simulation datasets of Harvzinski et al.[10, 11] A primary motivating element for these studies is to shed light on the fundamental interactions between the acoustic waves and the combustion heat release, which is a critical contributor to the development of combustion instabilities in this experiment in particular, and also in rocket injector flowfields in general.

II. Background

The decomposition analysis generally takes an ensemble of data, instantaneous or a series of snapshots, as inputs and uses a matrix processing technique called singular value decomposition (for POD) or the Arnoldi algorithm (for DMD). The decomposition of the original data sets is based on optimality for POD and frequencies for DMD. Both techniques result in modes which form an orthonormal basis. A detailed mathematical description of the POD technique is given by Chatterjee,[14] Berkooz et al.,[15] Cordier and Bergmann.[16] An introduction to DMD can be found in Rowley et al.[17] and Schmid.[18] An overview of the mathematical models of POD and DMD is given in the following sections.

A. Mathematical Model of Decomposition Techniques

The goal is to approximate a function, $z(x,t)$, over a domain of interest as a finite sum in the variables-separated form

$$z(x,t) \approx \sum_{k=1}^{M} a_k(t)\Phi_k(x) \tag{1}$$

with the reasonable expectation that the approximation becomes exact as M approaches infinity. Note that in Eq. (1) there is no fundamental difference between x and t, but we usually think of x as a spatial coordinate and t as the temporal coordinate.

The representation of Eq. (1) is not unique. For example, if the domain (experimental or computational) is a bounded interval X on the real line, then the functions $\Phi_k(x)$ can be chosen as a Fourier series, Legendre polynomials, Chebyshev polynomials, and so on. For different selections of the space-dependent function, $\Phi_k(x)$, the corresponding time-dependent function, $a_k(t)$, will be different. They can be periodic or non-periodic, single-frequency dominated or multi-frequency dominated.

In the POD analysis, the spatial functions, $\Phi_k(x)$, are chosen to be orthonormal functions, i.e.

$$\int_X \Phi_{k_1}(x)\Phi_{k_2}(x)dx = \begin{cases} 1 \text{ if } k_1 = k_2 \\ 0 \text{ otherwise} \end{cases} \tag{2}$$

Then

$$a_k(t) = \int_X z(x,t)\Phi_k(x)dx, \tag{3}$$

From Eq. (2) and (3), it is noted that, given that $\Phi_k(x)$ is selected to be orthonormal, the determination of $a_k(t)$ will be only dependent on $\Phi_k(x)$ rather than on other Φ functions.

B. Singular Value Decomposition (SVD) in POD Analysis

In practice, whole datasets or snapshots are arranged into a POD matrix first, for example, with each row containing the temporal data and each column containing the spatial data. Thus, if there are N rows of temporal data and m columns of spatial data, the POD matrix will be of size $N \times m$.

Once we obtain the POD matrix A, the singular value decomposition (SVD) can be defined as,

$$A = U\Sigma V^T \tag{4}$$

where U is an $N \times N$ orthogonal matrix, V is an m x m orthogonal matrix, and Σ is an $N \times m$ matrix with all elements zero except along the diagonal. The diagonal elements Σ_{ii} consist of $r = \min(N, m)$ nonnegative numbers σ_i, defined as the singular values of A. They are arranged in decreasing order and are unique.

In Eq. (4), let $U\Sigma = Q$. Then, $A = QV^T$. Letting q_k be the k^{th} column of Q and v_k be the k^{th} column of V, we write out the matrix product as

$$A = QV^T = \sum_{k=1}^{m} q_k v_k^T \tag{5}$$

Eq. (5) is the discrete form of Eq. (1). And we can obtain the matrix for each POD mode,

$$A_k = q_k v_k^T \tag{6}$$

In Eq. (6), A_k is defined as the k^{th} POD mode for matrix A and it is noted that A_k has the same dimensions as the matrix A. Moreover, the column matrix q_k can be interpreted as the temporal mode of the k^{th} POD mode, while the column matrix v_k represents the spatial mode. Here, we note that if the temporal mode q_k is obtained such that $U\Sigma = Q$, the spatial mode v_k would contain all normalized numbers and vice versa. Or, we can write Eq.(6) in this way,

$$A_k = u_k \sigma_k v_k^T \tag{7}$$

In Eq.(7), u_k is the k^{th} column of U and σ_k corresponds to the k^{th} singular value of matrix A, which can further be defined as the mode power or energy of the k^{th} POD mode.

C. Arnoldi Algorithm in DMD Analysis

In the case of the DMD analysis, in order to obtain single frequency dynamic modes, linear mapping is assumed from one snapshot to another. Suppose the data set is represented as a snapshot sequence,

$$V_1^N = \{v_1, v_2, v_3, ..., v_N\} \tag{8}$$

where v_i stands for the i^{th} flow field and $v_{i+1} = Bv_i$. The matrix B here represents the linear mapping matrix. Therefore,

$$V_1^N = \{v_1, Bv_1, B^2 v_1, ..., B^{N-1} v_1\} \tag{9}$$

Another assumption is that there exists a specific number *N*, beyond which the vector v_N can be expressed as linear combination of the previous vectors,

$$v_N = a_1 v_1 + a_2 v_2 + ... + a_{N-1} v_{N-1} \quad \text{or} \quad v_1 = V_1^{N-1} a + r \tag{10}$$

Hence,

$$BV_1^{N-1} = V_2^N = V_1^{N-1} S + r e_{N-1}^T \tag{11}$$

where,

$$S = \begin{pmatrix} 0 & & & & a_1 \\ 1 & 0 & & & a_2 \\ & \ddots & \ddots & & \vdots \\ & & 1 & 0 & a_{N-2} \\ & & & 1 & a_{N-1} \end{pmatrix} \tag{12}$$

Applying the eigenvalue decomposition for matrix *S*,

$$S = T^{-1} \Lambda T \tag{13}$$

where matrix *T* is the eigenvector matrix of *S*. Suppose a sufficient number of snapshots are used, the eigenvalues of *S* can well represent the eigenvalues of *A*, which contains the time-evolution information of the flowfield.

Similarly the dynamic modes corresponding to single frequency response can be constructed as,

$$\Psi = V_1^{N-1} T^{-1} \tag{14}$$

Similarly, the original data set can be decomposed into the form in Eq. (1),

$$V_1^{N-1} = \Psi T \tag{15}$$

where matrix Ψ contains the dynamic spatial information and matrix T contains the temporal evolutional information.

D. Test Problem

The detailed description of the geometry used in the present study has been given by Harvzinski et al.[10, 11] The simulation is concerned with the combustion instability in a continuously variable resonant chamber (CVRC). Here, the geometry used for the decomposition analysis is briefly introduced in Fig. 1. Decomposed hydrogen peroxide, as the oxidizer, enters from the left through the center oxidizer post. The fuel, gaseous methane enters just before the backstep connecting the post and the combustion chamber. When applying the decomposition analysis, information from the entire computational domain is used for post-processing. The domain can be separated into three regions: region I represents the oxidizer post where there is only cold flow, region II is the heat release zone, and region III is the combustion chamber. In the original simulation, the two-dimensional grid contained 200,000 grid points and the three-dimensional grid contained 5,000,000 grid points. Information is interpolated from the original fine grid to a coarser one to perform the decomposition analysis due to the large memory requirement of the decomposition techniques and the fact that the resolved boundary layer need not be included. Mean values of pressure and heat release are extracted before post-processing. Only the fluctuating portions of the pressure and heat release p' and q', are used and focus has been put on the results from three-dimensional simulation, which show good agreement with the experimental results.[13]

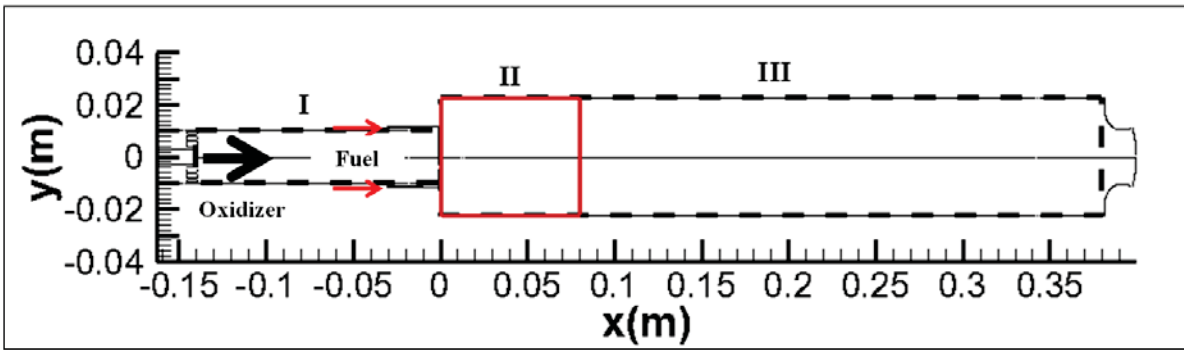

Figure 1. Test section overview including oxidizer post (I), heat release zone in the combustion chamber (II) and full combustion chamber (III).

Figure 2 shows the power spectral density (PSD) analysis of the raw pressure signals from the computational and experimental results.[10] The first six strongest acoustic frequencies can be observed from the figure. According to the computational results, the frequencies corresponding to the first six longitudinal pressure modes are 1540Hz (1L), 3090Hz (2L), 4636Hz (3L), 6182Hz (4L), 7692Hz (5L) and 9240Hz (6L) respectively. The experimental results indicate similar but slightly lower values.[13]

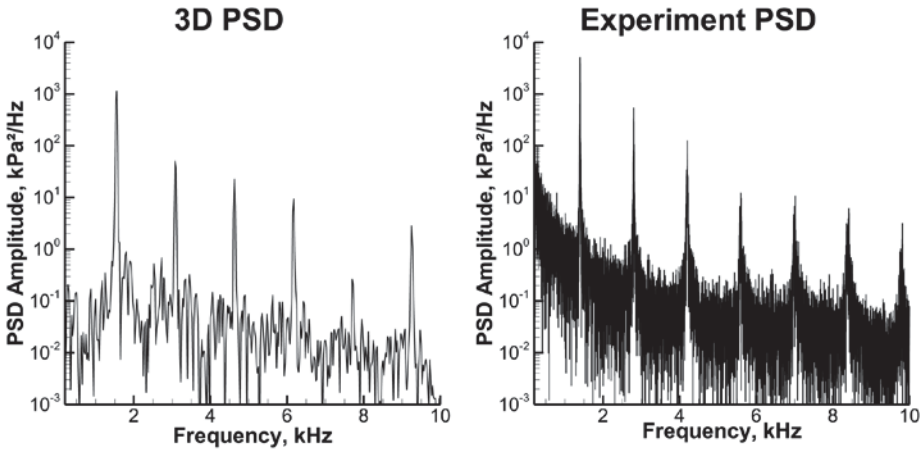

Figure 2. PSD Analysis for the raw pressure data showing the computational (left) and experimental results (right) from Harvazinski.[10]

Figure 3 shows the snapshots of some of the key flowfield quantities for one complete cycle, defined by the 1L frequency (1540Hz). Pressure contours along with the streamlines are shown on the top of each time instance. Heat release contour is shown on the bottom left with spatial mixture fraction and equivalence ratio contours shown on the bottom right. In the latter case, the fuel lean region (i.e., an equivalence ratio less than unity) has been blanked out in the contour plot. At the start of the cycle (i.e., 0° in Fig. 3), a strong pressure wave is observed coming from the oxidizer post to the backstep and two vortices are generated on the top and bottom of the post. As the vortices move downstream , they bring along fuel that mixes with the oxidizer. At the mid-point of the cycle (180° in Fig. 3), the vortices are further strengthened by the pressure wave coming upstream in the chamber, and the mixing of fuel and oxidizer is accelerated, which leads to strong heat release. As the pressure wave moves into the oxidizer post, the magnitude of the vortices decreases and so does the combustion heat release. Clearly the acoustics and combustion are well correlated with the significant heat release occurring when the pressure is high at the combustor head-end.

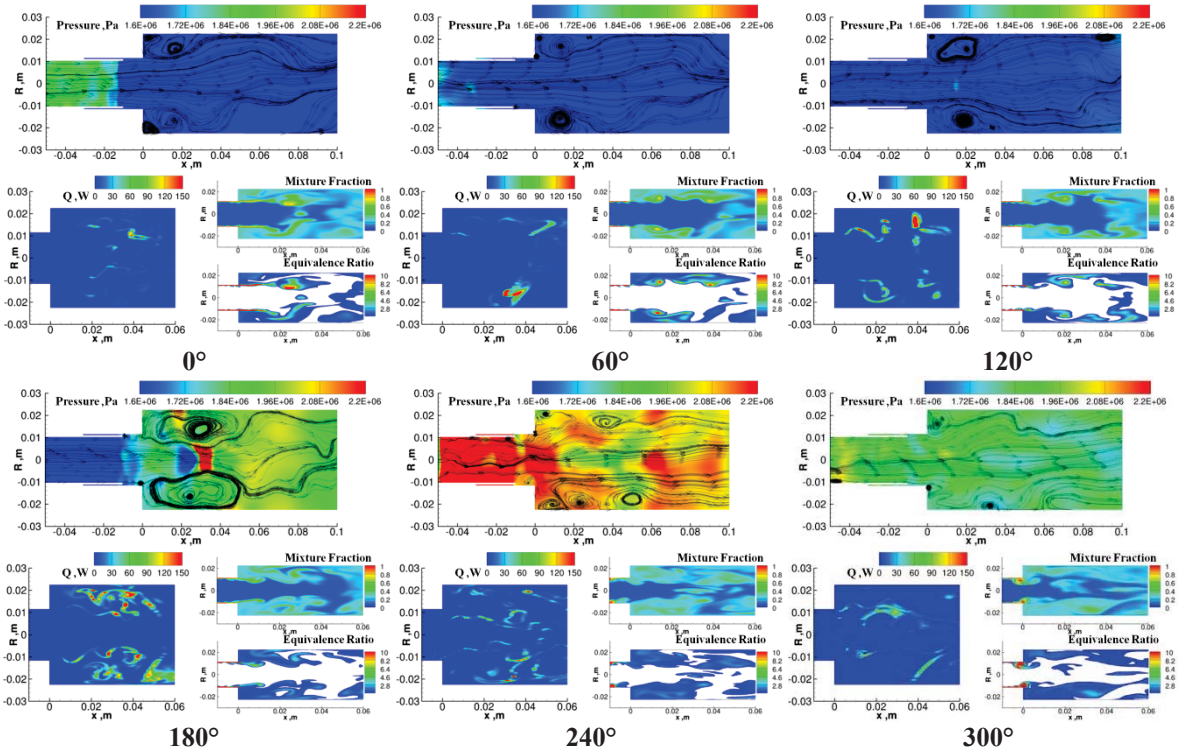

Figure 3. Instantaneous results of CVRC over one cycle (based on first longitudinal frequency).

III. Results

The experimental-computational comparisons of the CVRC data by Feldman et al.[13] show that the three-dimensional simulations are a better match to the experiments than the two-dimensional axisymmetric simulations, which under-predict the amplitude of the pressure oscillations. Detailed results using traditional filtering analysis are available in Harvazinski et al. [10] and the following section provides a brief overview. The rest of the discussion focuses on the use of POD and DMD techniques to shed light on the 3D simulation results.

A. Results using Traditional Filtering Techniques

Acoustic and heat release mode shapes are computed by dividing the computational domain into vertical strips (or discs in the three-dimensional case). Pressure and heat release are volume averaged in each strip. At the conclusion of the simulation, the data stored in each strip are filtered at the frequencies identified in the PSD plot and then sampled at a fixed interval. The sampled data are then in space plotted to show the mode shape for each filtered frequency.[10]

Figure 4 shows the pressure mode shapes for 1L, 2L and 3L frequencies and the results show the classical mode shapes in the chamber, while the mode shape in the oxidizer post appears to be accommodate the choked condition at the inlet as well as the area transition that occurs at the back-step.

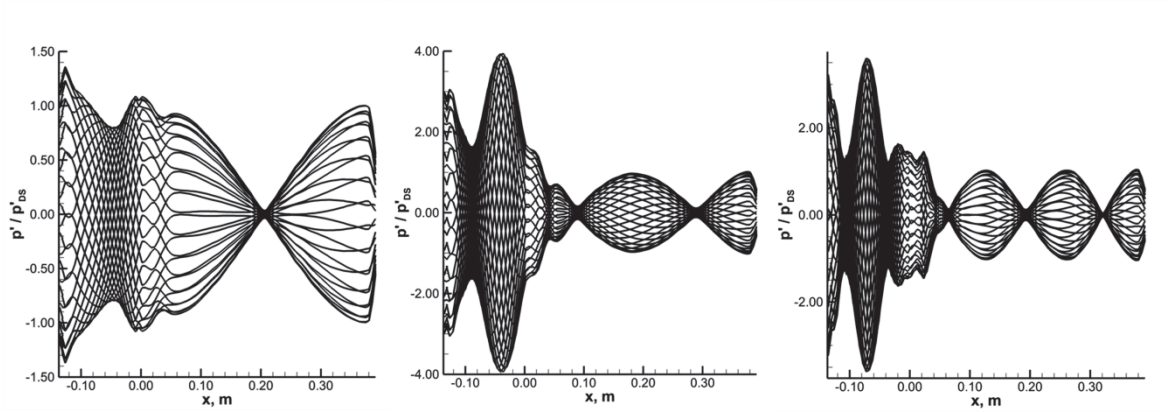

Figure 4. Pressure mode shapes obtained by filtering around 1L (left), 2L (middle) and 3L (right) frequencies from Harvazinski.[10]

Figure 5 shows the heat release mode shapes. The first three modes are dominant and show that the peak heat release is concentrated near 0.04m downstream from the backstep. For the 1L mode a single peak is observed. For the2L mode an additional small peak appears just downstream of the backstep, while for the 3L, yet another peak appears downstream of the dominant peak.

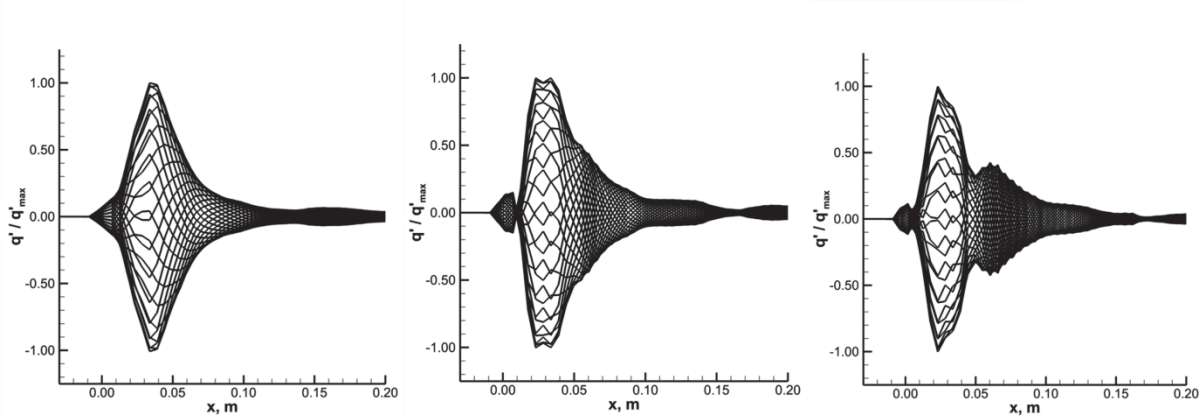

Figure 5. Heat release mode shapes obtained by filtering around 1L (left), 2L (middle) and 3L (right) frequencies from Harvazinski.[10]

B. POD Results

Figure 6 shows the POD mode power as a function of the mode number. We note that the mode power is given by the value of σ_k in Eq.(7), which indicates the significance of each POD mode. The POD mode power distribution of *p'* has a sharp decrease after the first mode and decays to zero very quickly as the mode number increases. However, the power distribution of the *q'* mode is different in that it decreases much more gradually. The first POD mode of *p'* contains 11% of the total information while that of *q'* has only 0.66%. In the figure, the summation of first 200 POD modes of *p'* and *q'* are given by the solid line. For *p',* the first 200 modes account for approximately 55% of the energy, while for *q',* the first 200 modes account for only about 22% of the energy. This indicates that more POD modes of *q'* are need to fully represent the behavior of the heat release rate. The source of this behavior can be examined by looking at the PSD plot, shown in Fig. 7. In particular, the PSD of the heat release perturbations shows lower power at the dominant frequencies, which may be attributed to the richer characteristics of the combustion process compared with the acoustic response which is more predictable and organized.

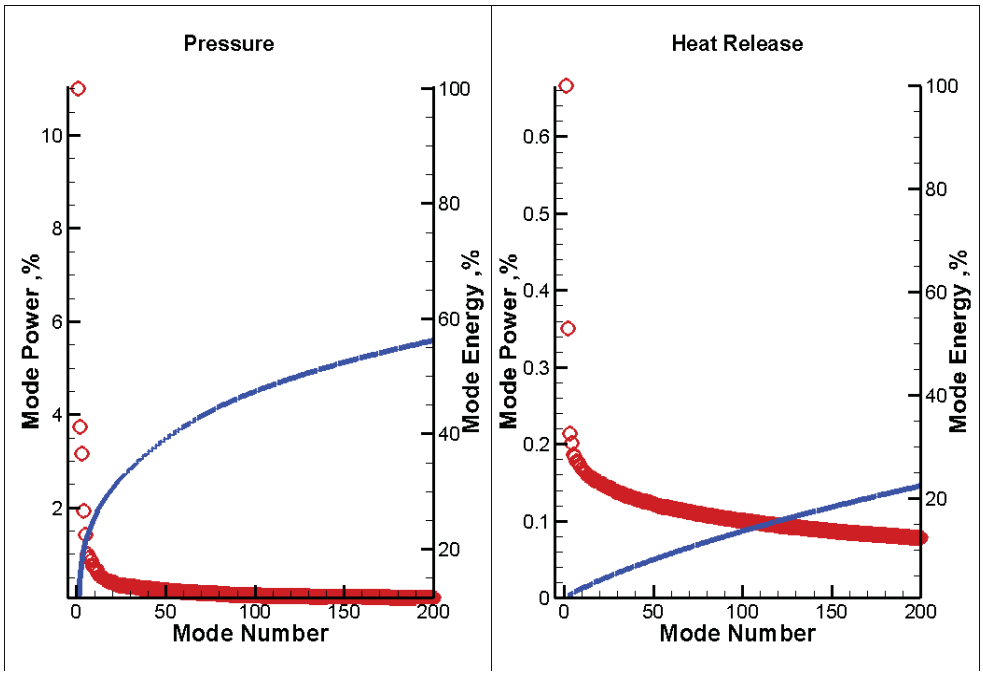

Figure 6. POD mode power and accumulated energy of pressure oscillations (left) and heat release oscillations (right).

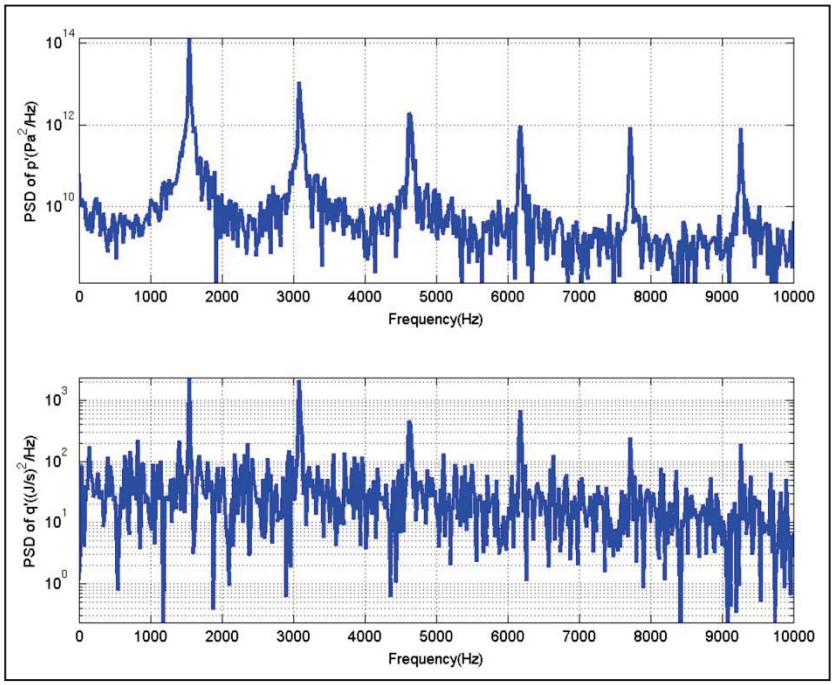

Figure 7. Power spectral density of pressure (top) and heat release (bottom) oscillations near the location of maximum heat release.

In the next two sections, mode shapes of the pressure and heat release oscillations as given by the POD analysis are discussed. Both the spatial contours and temporal modes are shown for each POD mode. Since only the fluctuation terms are included in the decomposition analysis, negative values shown in the figures below indicate a decrease in magnitude relative to the mean and vice versa.

a. POD Modes of Pressure Oscillations

The first six POD modes of the pressure oscillations for the combined combustion chamber and oxidizer post configuration are shown in Figs. 8-10. In each case, we show the spatial modes (top) as well as the temporal mode and the PSD of the temporal mode (bottom). Contours of the POD spatial modes are plotted on a slice which goes through the center of the domain. Figure 8 shows that the dominant frequency is 1550Hz which corresponds to the first longitudinal mode. The first POD mode is also subject to minor influences from the 2L, 3L, 4L, and 5L acoustic modes as evident in the PSD plot of temporal mode.

Multiple frequencies continue to appear in the higher POD modes. The higher POD modes tend to be dominated by the higher acoustic frequencies present in the chamber. This is consistent with the energy distribution plot shown in Fig. 6. Since the POD is designed to obtain an optimal representation of the original data set, it can be concluded that the proper description of the acoustic responses within the computational geometry is complex and cannot be approximated using a single frequency. Instead, a combination of multiple frequencies is required. Even though the same frequencies appear in multiple temporal POD modes, their relative contributions are different for each mode because of the different spatial modes present. For instance, the 3rd and 4th POD modes in Fig. 9 is dominated by the 2L and 3L modes, while the 5th POD mode in Fig. 10 is dominated by the 3L, 4L and 5L modes and the 6th POD mode (also in Fig. 10) is dominated by the 5L and 6L modes.

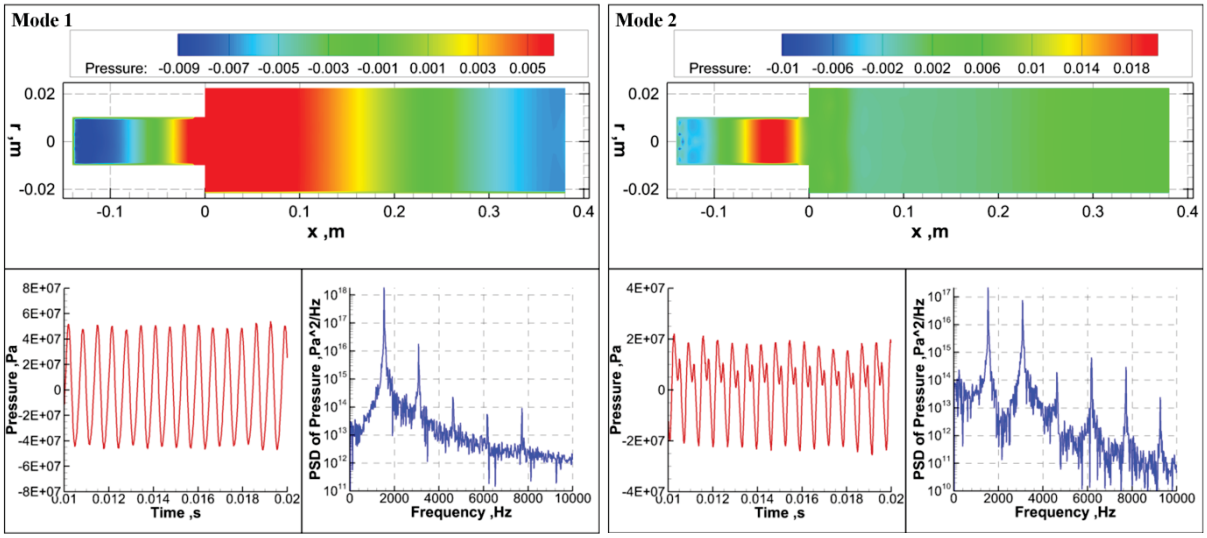

Figure 8. POD analysis of pressure oscillations from 3D simulations with 1st mode (left), 2nd mode (right).

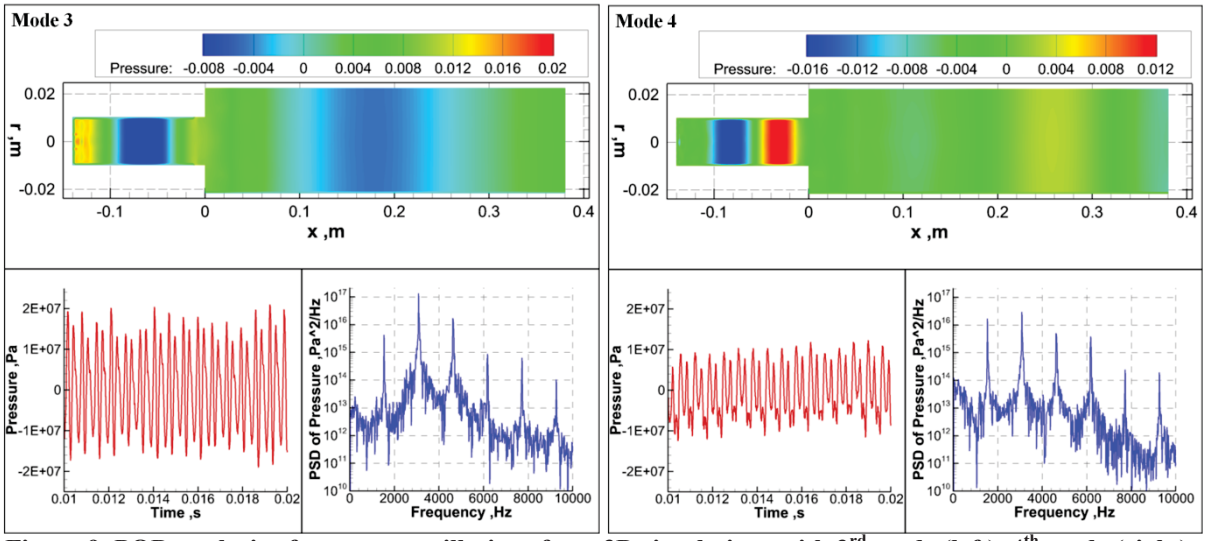

Figure 9. POD analysis of pressure oscillations from 3D simulations with 3rd mode (left), 4th mode (right).

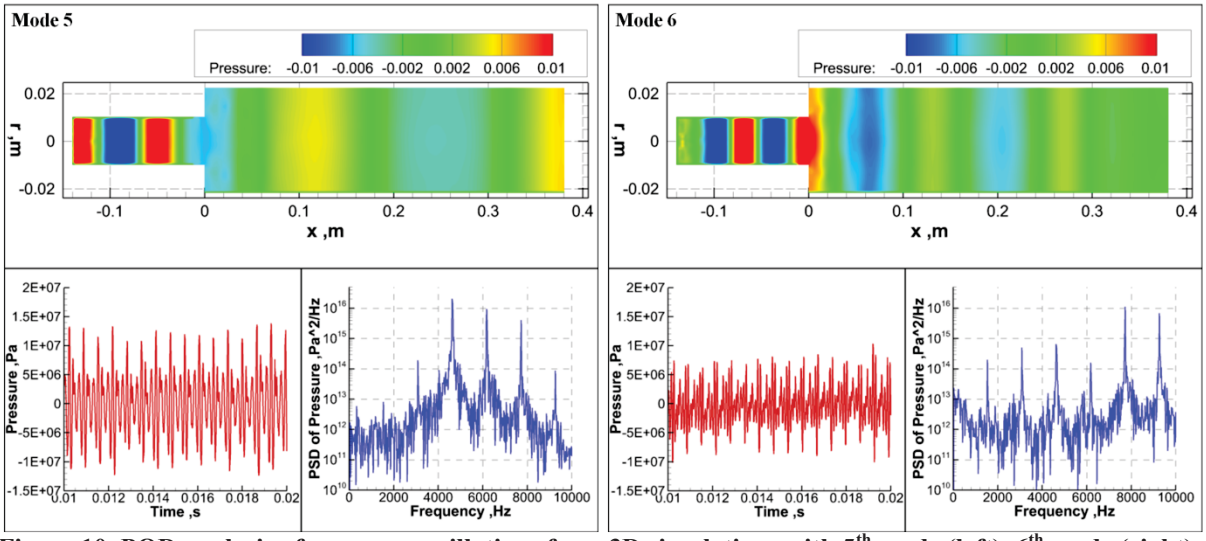

Figure 10. POD analysis of pressure oscillations from 3D simulations with 5th mode (left), 6th mode (right).

b. POD Modes of Heat Release Oscillations

The first six POD modes of heat release oscillations are shown in Figs. 11 - 13. Again, in each case, we show the spatial mode as well as temporal mode and the PSD of the temporal mode. Most of the combustion occurs in section II (i.e., the heat release zone in Fig. 1) and, for this reason, the heat release POD modes are shown only for this section. The first POD mode of the heat-release in Fig. 11 shows a combustion pulse between 0.03 and 0.04m. The second heat-release POD mode shows a half-wave configuration in terms of the spatial mode contour. As in the case of pressure, each POD mode is, in fact, a combination of longitudinal mode frequencies. The frequency values correspond to the pressure modes very well; however, the specific combination of longitudinal modes in each case is different from the pressure case.

It is interesting that the combustion heat release in the 1st POD mode in Fig. 11 appears to come from the main vortex in Fig. 3, which we noted earlier is strengthened by the incoming pressure wave. This vortex accelerates the mixing of fuel and oxidizer and promotes the heat release. Moreover, the location where the vortex meets the strong pressure wave is consistent with the location of the heat-release spatial mode. This result is therefore a clear indication of the combustion-pressure coupling that plays a critical role in generating and sustaining the combustion instabilities. As the vortex moves downstream, it starts to be influenced by the additional acoustic modes, which separates the single main vortex into several smaller ones. This can be observed from the 2nd POD mode also shown in Fig. 11. Here. an additional combustion heat-release zone appears further downstream, which is opposite in phase with the primary heat-release location. As shown in the PSD plot in 1st and 2nd POD modes in Fig. 11, these two combustion modes are highly responsive to the first three acoustic modes. Thus, the two combustion modes appear to represent the major combustion dynamics fluctuations that we observed earlier in Fig. 3.

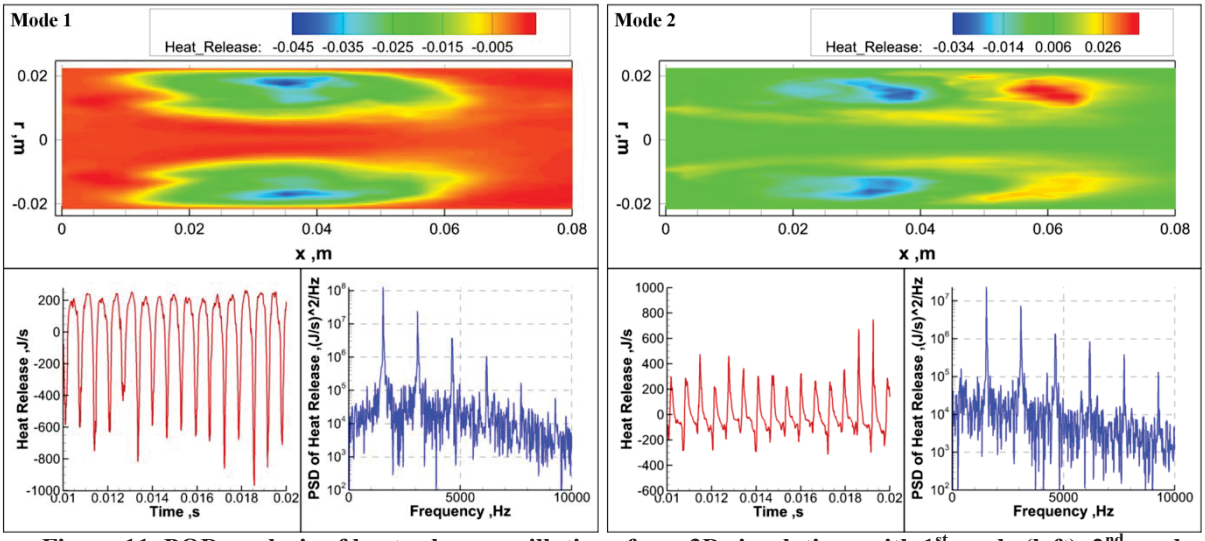

Figure 11. POD analysis of heat release oscillations from 3D simulations with 1st mode (left), 2nd mode (right).

After the high amplitude pressure wave passes through the chamber and enter the post, higher acoustic modes with lower magnitudes come into play, perhaps influenced by the dynamics in the post. These higher modes lead to additional vortex splitting and in turn lead to lower amplitude combustion fluctuations, which are captured by the 3rd and 4th POD modes in Fig. 12. These two modes describe the downstream transition of the smaller-scale combustion and, moreover, they suggest an extra upstream combustion location. In Fig. 3 (at 240° and 300°), small vortices are observed to be pushed upstream towards the backstep by the upcoming pressure waves. This results in enhanced mixing of fuel and oxidizer near the backstep location. Moreover, the PSD plots indicate that the 4L, 5L and 6L modes are dominant in these combustion responses. Further description of the role of longitudinal frequencies in the combustion dynamics is discussed later in section C as part of the DMD analysis.

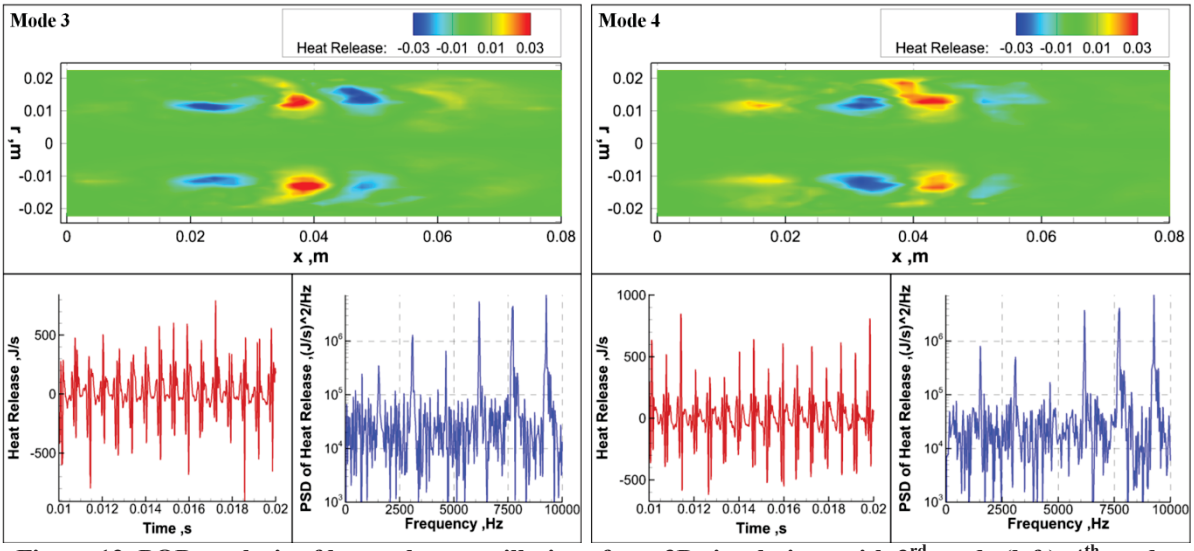

Figure 12. POD analysis of heat release oscillations from 3D simulations with 3rd mode (left), 4th mode (right).

The 5th and 6th POD mode of the heat release in Fig. 13 do not suggest a strong repeatable behavior in terms of the temporal modes shown in the bottom left although they show some peaks around 1L, 2L and 3L frequencies in terms of the PSD plots in bottom right. Moreover, the spatial modes do not indicate a predictable pattern as do the first four POD modes. In fact, there is some evidence of radial or azimuthal modes in these patterns which should be investigated further.

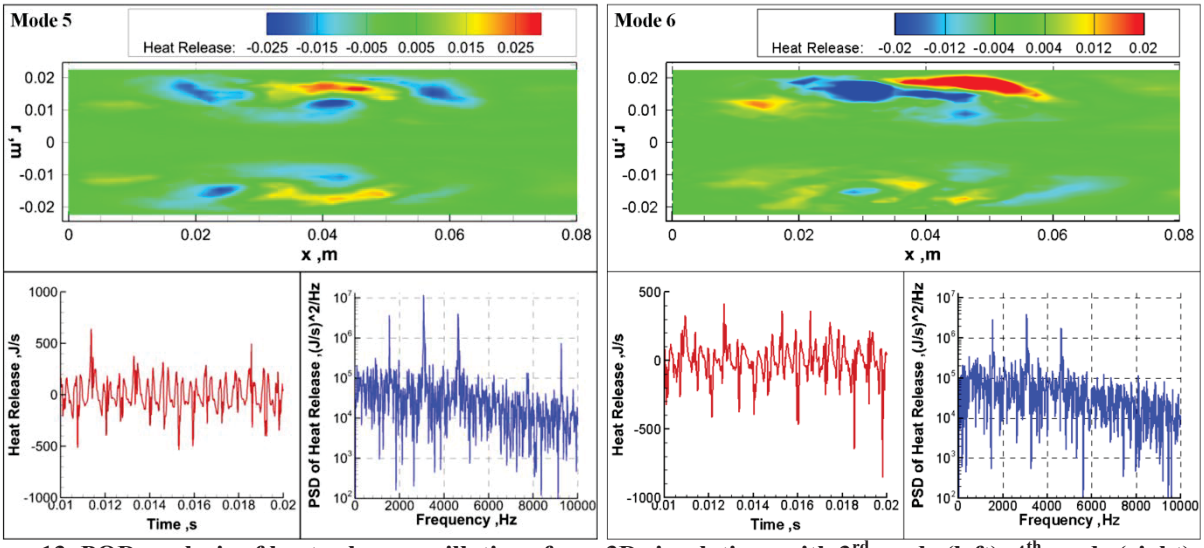

Figure 13. POD analysis of heat release oscillations from 3D simulations with 3rd mode (left), 4th mode (right).

Although in terms of the POD mode power spectrum in Fig. 6, the heat release oscillations require a large number of POD modes, we note that the primary combustion response is captured by the first few POD modes. The higher POD heat modes can be regarded as representations of spontaneous and chaotic combustion processes which are not necessarily coupled with the acoustic modes. This indicates that focusing on the lower POD heat release modes is sufficient to shed insight into the physical phenomena of relevance to combustion stability.

C. DMD Results

Unlike the POD analysis, the DMD technique provides modes at discrete frequencies. Figure 14 shows the DMD mode power versus frequencies allowing the importance of each frequency to be determined. Both pressure and heat-release modes are shown. As expected, the heat release oscillations show strong response to the longitudinal acoustic frequencies. But, other than the expected acoustic frequencies, there are also additional peaks of lower magnitude in the high frequency region from 10,000 to 20,000 Hz. This confirms what has been concluded previously from the POD mode results, that in addition to the pressure mode response, the combustion dynamics also contains additional physics that can be characterized as the result of the turbulent reacting flowfield.

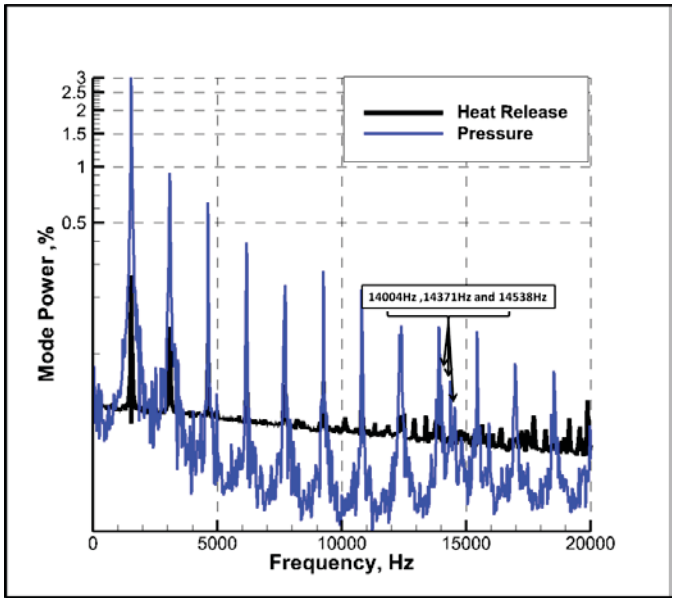

Figure 14. DMD mode power.

Mode studies of the pressure and heat release oscillations using DMD analysis are shown in Figs. 15 - 17.We note that the DMD temporal modes are very simple since they include only a single frequency. For this reason, only spatial modes are shown. The pressure modes produced by the DMD are immediately recognizable and look like the acoustic modes one would expect in the chamber. Figure 15 shows the DMD pressure modes for the first two longitudinal modes. In the combustor, the first mode is a half-wave and the second mode is a full-wave. The mode shapes within the oxidizer plot are slightly more complicated but also correspond to the above trend. Specifically, the combined mode shapes also correspond to the band-passed one-dimensional mode shapes derived in Fig. 4.

DMD modes of the heat release oscillations in response to 1L and 2L acoustic frequencies in Fig. 15 appear to give similar interpretations as in the case of the POD results given in Fig. 11. Importantly, the 1L DMD heat-release mode shows a pulsating response near 0.04m, which confirms that this response is mainly driven by 1L acoustic frequency. The 2L DMD heat release mode demonstrates that the combustion starts to function in alternate locations, both upstream and downstream of the primary response region of the first mode. We note that, in contrast, the POD modes represent the response to a combination of acoustic modes and, therefore, it is difficult to discern the precise driving mechanisms. Thus, the DMD analysis provides more precise mode-by-mode representation of the driving mechanisms and is therefore a more quantitative approach than the POD analysis.

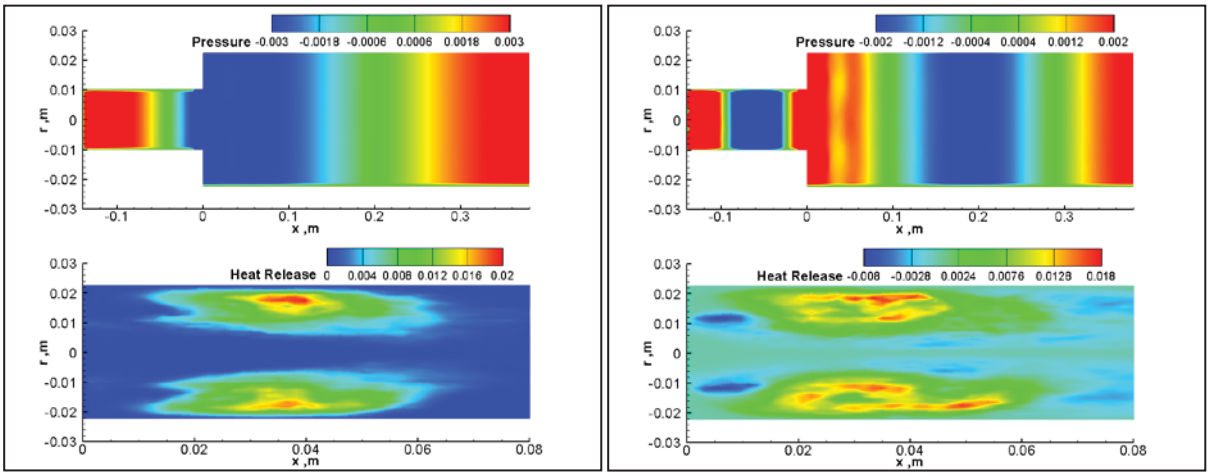

Figure 15. DMD modes of pressure and heat release with 1L frequency (left) and 2L frequency (right).

When it comes to responses to higher acoustic frequencies shown in Fig. 16 and Fig. 17, the DMD analysis gives the expected pressure mode shapes in the combustion chamber (one and half waves for 3L, two full waves for 4L, two and half waves for 5L and three full waves for 6L) while in the oxidizer post, there appear to be some evidence of mode-shifting with the modes in the chamber. For example, the DMD pressure mode of the 3L frequency shows a full wave in the oxidizer post. This lack of tuning might be attributed to the different sound speeds in the chamber and the oxidizer post because of the lower temperature of the unburned propellants in the post.

The 3L DMD heat-release mode in Fig. 16 (left) suggests a similar spatial configuration as the 2L DMD heat-release mode. This indicates that the 2L and 3L frequencies contribute significantly to the alterations of the combustion processes between 0 m and 0.08m in the chamber while the response driven by the 1L frequency is centered at 0.04m. The higher DMD heat release modes in Fig. 16 (right), Fig. 17 (left) and Fig. 8 (right) show similar results although the heat release zones are observed to be more compact presumably because of the higher frequencies (and, consequently shorter wavelengths) involved.

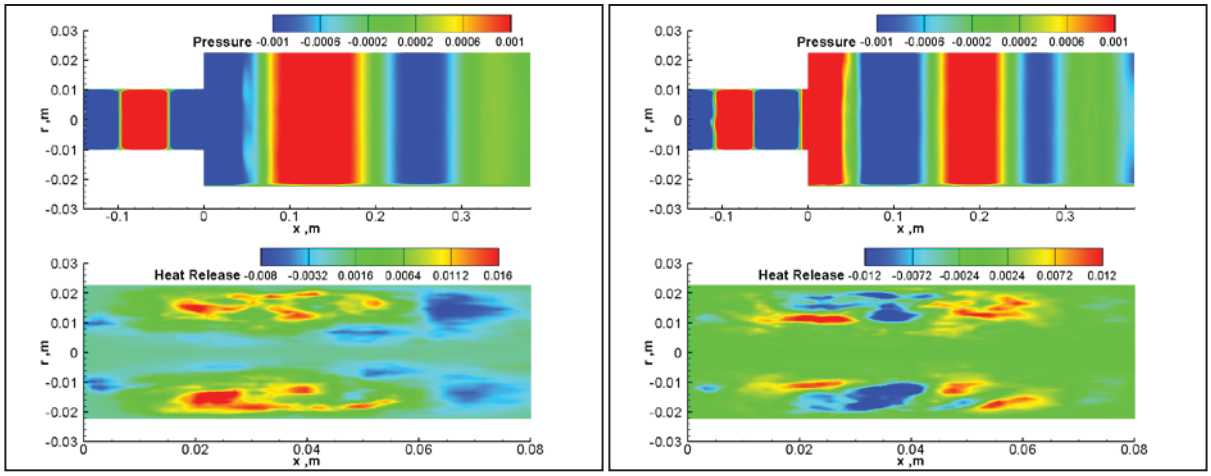

Figure 16. DMD modes of pressure and heat release with 3L frequency (left) and 4L frequency (right).

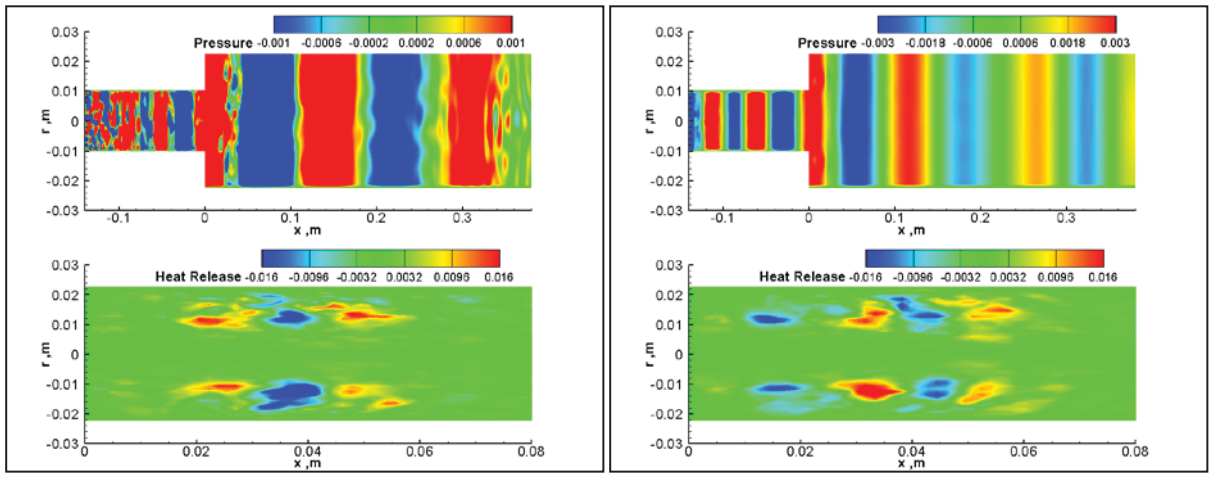

Figure 17. DMD modes of pressure and heat release with 5L frequency (left) and 6L frequency (right).

Other than the longitudinal acoustic frequencies discussed so far, the DMD analysis also indicates three lower amplitude peaks between the longitudinal frequencies, highlighted in the spectrum in Figure 14 at 14004, 14371 and 14538 Hz respectively. Spatial contours in response to these three frequencies are shown in Figure 18. In terms of the pressure contours, 14004Hz corresponds to the 1st tangential (1T) acoustic mode, 14371Hz appears to show the 1T2L mode, and 14538Hz appears to correspond to the 1T3L mode. These tangential modes can be theoretically described by the linear wave equation but have not been previously observed in the CVRC simulations using traditional data-processing techniques. Heat release in response to these high frequencies is dominated by small scale combustion, which may be more related to turbulence than acoustics. In fact, the DMD spectrum displays no strong peaks for the heat release at these frequencies, which allows us to conclude that the tangential acoustic modes play weaker role in influencing combustion than do the longitudinal modes. Nevertheless, these results demonstrate the capability of the DMD analysis to shed light on underlying physical phenomena that are not otherwise evident.

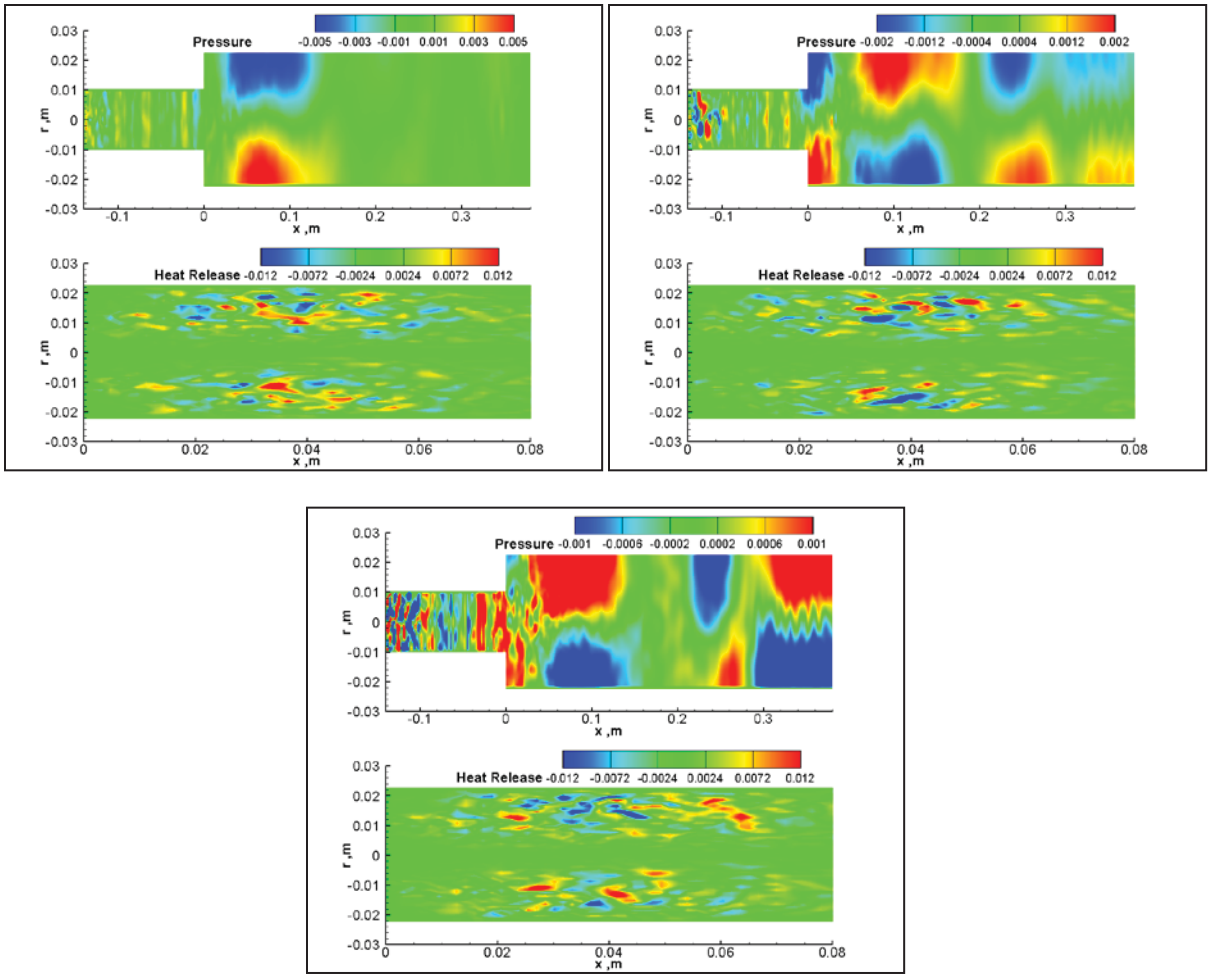

Figure 18. DMD modes of pressure and heat release with 14004Hz (top left), 14371Hz (top right) and 14538 Hz (bottom).

At this point, we can also draw some conclusions on the relative utility of the POD and DMD analysis. The POD technique is designed to extract the representative dynamic modes out of the original dataset or snapshots. It offers a mathematically optimal lower-order approximation of the original high-order system and therefore may provide a good quantitative understanding of the observed phenomena. Connections between frequencies can be studied because in most cases, the POD modes are multi-frequency driven. However, the couplings between different variables, such as pressure and heat release, are not easily determined. Specifically, the POD modes for pressure and heat release do not have a one-to-one correspondence and may in general contain the responses to different underlying mode structures. On the other hand, the DMD technique provides more quantitative interpretations of the response to a specific frequency. Pressure and heat release can be coupled easily on the basis of frequencies, which can be helpful in developing fundamental insight into the coupling mechanisms responsible for driving the instabilities. Moreover, the approach can be useful for developing appropriate transfer functions between the acoustics and the combustion, which can be used in lower-order engineering models of combustion instability.

D. Applications of Decomposition Techniques in Calculating Rayleigh Index

The Rayleigh index is defined as the degree of correlation between the pressure and the combustion heat release. The Rayleigh criterion states that when the pressure and heat release are in-phase (i.e., a positive Rayleigh index), combustion instabilities are driven, while when they are out-of-phase (i.e., a negative Rayleigh index), combustion instabilities are damped. The Rayleigh index is therefore a useful diagnostic tool for obtaining a quantitative understanding of combustion instability incidence. Previous studies of the Rayleigh index are based on filtered signals around the concerned acoustic frequencies as reported by Harvazinski et al.[19] Sample three-dimensional

results of the Rayleigh index using filtered data for the first three acoustic frequencies have been analyzed by Harvazinski[10] and are reproduced in Fig. 19. We will discuss these trends in the context of similar results obtained using the POD and DMD analysis.

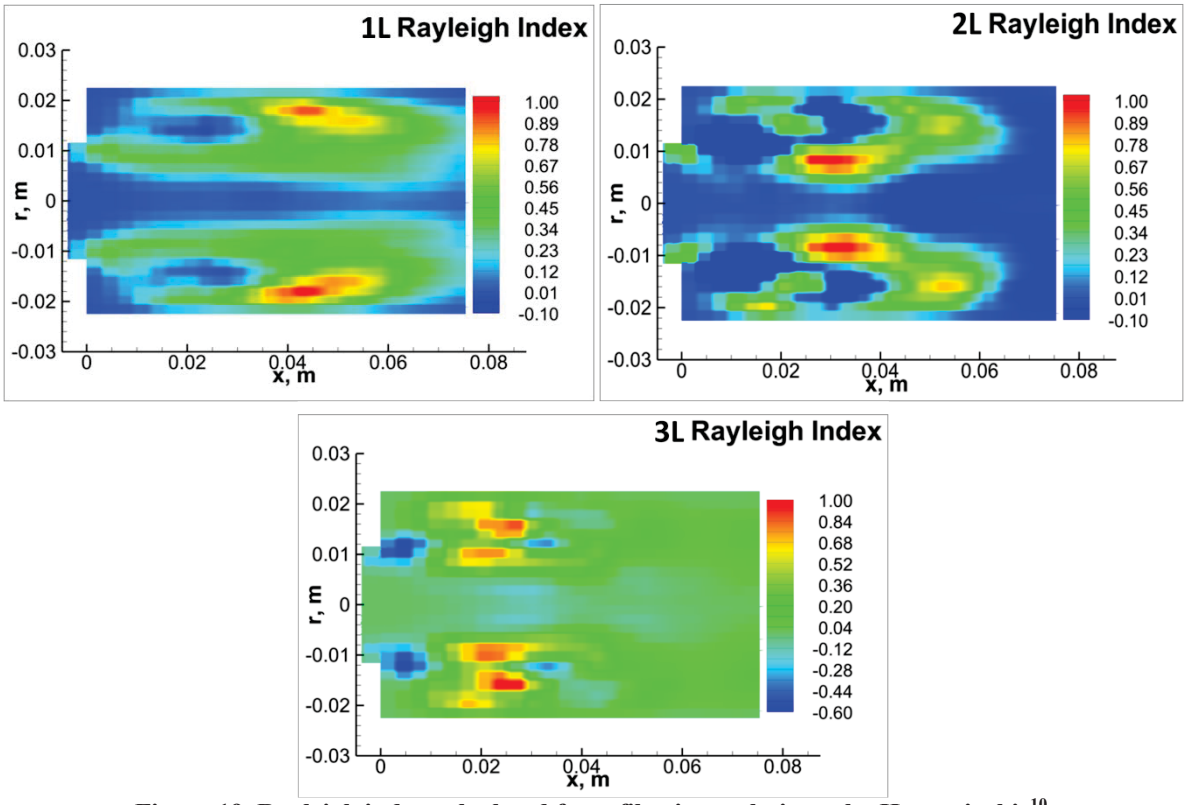

Figure 19. Rayleigh index calculated from filtering techniques by Harvazinski. [10]

The Rayleigh index calculated from the POD modes is shown in Fig. 20. Because the decomposition analysis is performed independently for each variable (*p'* and *q'*), it is hard to correlate pressure and heat release oscillations using the POD results. As discussed above, each POD mode does not necessarily correspond to a single frequency. Therefore, to calculate the Rayleigh index from the POD modes, the non-filtered raw signal of heat release oscillations is used rather than the filtered or decomposed ones. Moreover, the decomposed pressure POD modes are used in terms of the dominant frequencies. Based on the results in Figs. 8 - 10, the 1st ,3rd and 5th POD pressure modes have dominant responses from the 1L, 2L and 3L acoustic frequencies respectively. For this reason, we select these three POD modes to derive the Rayleigh index. In Fig. 20, the contour scales are normalized by the strongest Rayleigh index magnitude, which comes from 1st POD mode of pressure in these three cases.

Comparing the results in Fig. 19 and Fig. 20, the Rayleigh index due to the 1st POD pressure mode (which is mainly driven by 1L frequency) gives similar interpretations of the combustion heat-release mechanism. A dominant driving region lies downstream near the 0.04 m location with a small damping region sitting close to 0.02m. The corresponding results for the 3rd POD mode shows that the maximum Rayleigh index is only 10% compared to the first mode result; however, it shows the same locations for the strongest driving and damping regions as do the filtered results in Fig. 19. Finally, the Rayleigh index results for the 5th POD pressure mode appear to be similar to the 3L filtered Rayleigh index with a relatively low damping region near the inlet (backstep) and a strong driving area 0.02m downstream.

Unlike the POD modes, the DMD modes of the pressure and heat release oscillations can be correlated by frequency. Figure 21 shows the Rayleigh indices based on the DMD modes corresponding to the 1L, 2L and 3L acoustic frequencies. Comparing the results shown in Fig. 19, Fig. 20 and Fig. 21, the Rayleigh index driven by 1L frequency predicts a single dominant driving location centered around 0.04 m, except that in the filtered results, the location is slightly downstream in the filtered case. The 2L and 3L DMD Rayleigh indices are also qualitatively similar to the results observed in the filtering and POD analysis in that they predict approximately the same locations for driving and damping mechanisms.

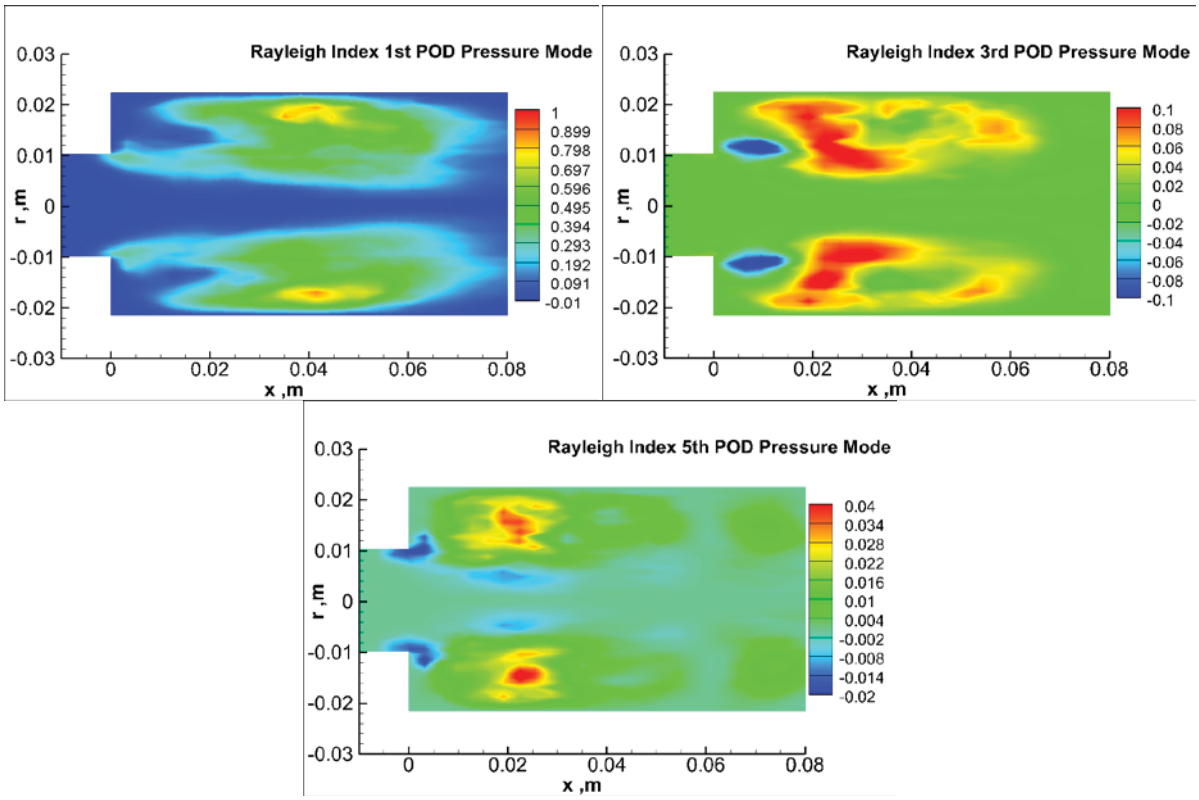

Figure 20. Rayleigh index calculated from POD modes.

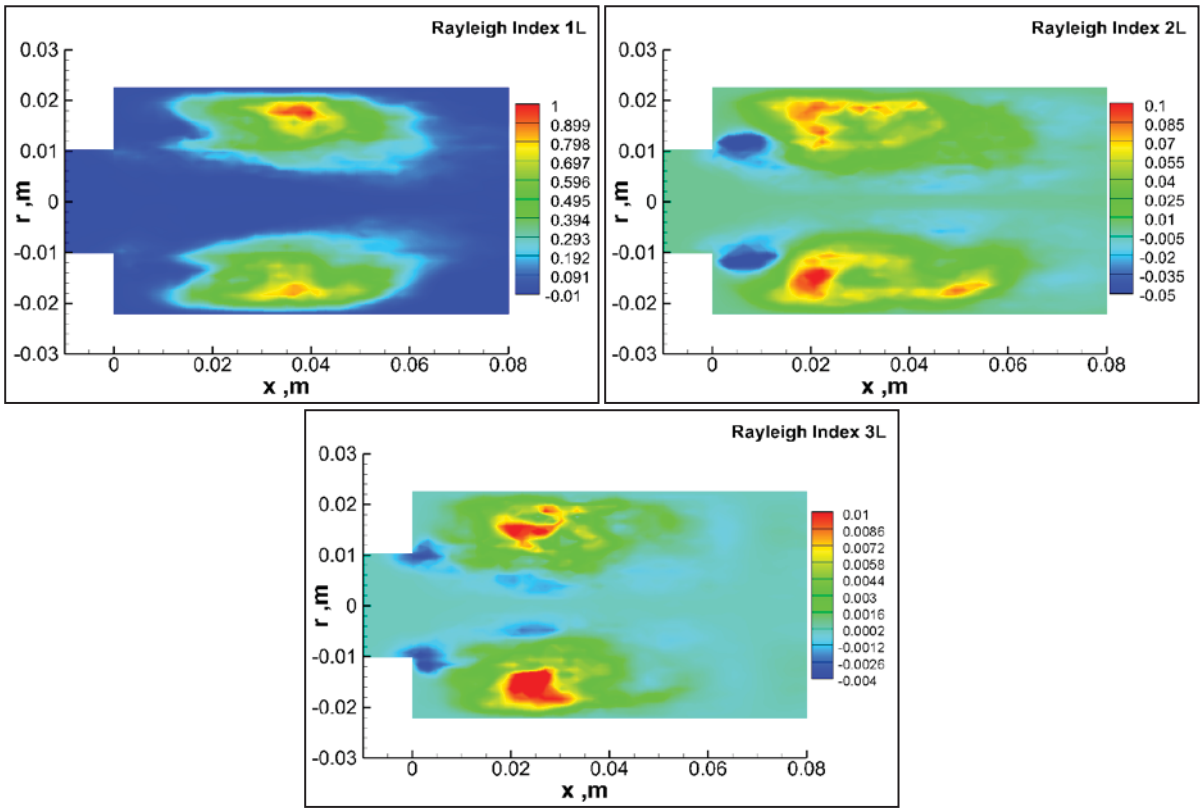

Figure 21. Rayleigh index calculated from DMD modes.

Overall, the Rayleigh index results given by the DMD analysis are qualitatively similar to the filtered results, but they are not identical. This is because when filtering the signals, the results can be influenced by the way the signals are processed. For example, different bandwidths, different types of filtering windows or different orders of filtering can influence the results. Therefore, filtering cannot precisely ensure a purely single-frequency response. In that respect, the DMD results are perhaps the most reliable way to quantify such effects.

IV. Conclusions

This paper is concerned with the analysis of three-dimensional simulation results for self-excited combustion instabilities in a longitudinal mode rocket chamber. Both proper orthogonal decomposition (POD) and dynamic mode decomposition (DMD) techniques are used as data-processing methods. The overall goal is to use these techniques to shed light on the fundamental coupling mechanisms between the chamber acoustics and the combustion dynamics and to thereby understand the driving mechanisms that promote the incidence of combustion instabilities.

POD analysis provides a series of POD modes of decreasing energy content. However, each of the modes correspond to a mix of acoustic modes and, moreover, there is no direct connection between the individual pressure and heat release modes. These factors make the POD analysis more useful as a means of lower-order representation of the solution, but the analysis is more limited in terms of establishing a quantitative basis for the combustion-acoustic coupling mechanisms. The frequency-based DMD technique, on the other hand, provides modes that correspond to single frequencies. Moreover, the corresponding pressure and heat-release modes contain useful information regarding how these two variables are coupled to each other and therefore provide a more quantitative basis for understanding combustion instability.

In terms of the heat release fluctuations, both POD and DMD analysis clearly reveal a dominant pulsating combustion mode, which is driven mainly by the 1L acoustic mode. The corresponding Rayleigh index derived from the DMD analysis shows that this combustion response is in phase with the pressure and leads to a strong positive Rayleigh index that is centered around the 0.04 m location downstream of the back-step. The 2L and 3L DMD heat release modes show that there are additional combustion response locations on either side of the dominant mode. The corresponding Rayleigh index reveals both damping and growth regions, although the growth regions are considerable weaker than that obtained for the 1L mode. This is to be expected since the present case corresponds to a 1L mode instability in the chamber.

Future work will include extending these studies to more stable regimes of combustor operation and using the POD and DMD analyses to predict the damping mechanisms that are dominant under stable operating conditions. Further, the use of DMD analysis to derive combustion response functions will also be investigated.

References

[1] Bouhoubeiny, E., Druault, P., and Mecanique, C.R., "Note on the POD-based time interpolation from successive PIV images", *Academie des sciences*, 2009.

[2] Shi, L., Liu, Y., Wan, J., "Influence of wall proximity on characteristics of wake behind a square cylinder: PIV measurements and POD analysis", *Experimental Thermal and Fluid Science*, Vol. 34, 2010, 28-36.

[3] Iudiciani, P., Duwig, C., Hosseini, S.M., Szasz, R.Z., Fuchs, L., Gutmark, E.J., Lantz, A., Collin, R. and Alden, M., "Proper Orthogonal Decomposition for experimental investigation of swirling flame instabilities", *48th AIAA Aerospace Science Meeting including the New Horizons Forum and Aerospace Exposition*, 4-7 January 2010.

[4] Huang, Y., Wang, S., and Yang, V., "Systematic Analysis of Lean-Premixed Swirl-Stabilized Combustion", *AIAA JOURNAL*, Vol. 44, No.4, April 2006.

[5] Zong, N., and Yang, V., "Supercritical Fluid Dynamics of Pressure Swirl Injector with External Excitations", *43rd AIAA/ASME/SAE/ASEE Joint Propulsion Conference & Exhibit*, 8-11 July 2007.

[6] Iudiciani, P., Duwig, C., Hosseini, S.M., Szasz, R.Z., Fuchs, L., and Gumark, E.J., "Proper Orthogonal Decomposition for Experimental Investigation of Flame Instabilities", *AIAA JOURNAL*, Vol. 50, No. 9, September 2012.

[7] Seena, A., and Sung, H.J., "Dynamic mode decomposition of turbulent cavity flows for self-sustained oscillations", *International Journal of Heat and Fluid Flow*, Vol. 32, 2011, pp. 1098-1110.

[8] Muld, T.W., Efraimsson, G., and Henningson, Dan S., "Flow structures around a high-speed train extracted using Proper Orthogonal Decomposition and Dynamic Mode Decomposition", *Computers & Fluids*, Vol. 57, 2012, pp. 87-97.

[9] Kalghatgi, P and Acharya, S, "Modal Analysis of Countercurrent Shear Flows", *42nd AIAA Fluid Dynamics Conference and Exhibit*, 25-28 June 2012, New Orleans, Louisiana.
[10] Harvazinski, M.E., "Modeling Self-Excited Combustion Instabilities Using A Combination of Two- and Three-Dimensional Simulations", Ph.D. dissertation, Mechanical Engineering Dept., Purdue University, West Lafayette, IN, 2012.
[11] Harvazinski, M.E., Xia, G., Anderson, W.E., and Merkle, C.L, "Analysis of Self-Excited Combustion Instability using a Combination of Two- and Three-Dimensional Simulations", *50th AIAA Aerospace Science Meeting including the New Horizons Forum and Aerospace Exposition*, 09-12 January 2012, Nashville, Tennessee.
[12] Garby, R., Selle, L., and Poinsot, T., "Analysis of the impact of heat losses on an unstable model rocket-engine combustor using Large-Eddy Simulation", *48th AIAA/ASME/SAE/ASEE Joint Propulsion Conference & Exhibit*, 30 July – 01 August 2012, Atlanta, Georgia.
[13] Feldman, T.W., Harvazinski, M.E., Merkle, C.L., and Anderson, W.E., "Comparison Between Simulations and Measurement of Self-Excited Combustion Instability", *48th AIAA/ASME/SAE/ASEE Joint Propulsion Conference & Exhibit*, 30 July – 01 August 2012, Atlanta, Georgia.
[14] Chatterjee, A, "An introduction to the proper orthogonal decomposition", *Current Science*, Vol. 78, No. 7, 10 April 2000.
[15] Berkooz G., Holmes P., and Lumley J.L., "The Proper Orthogonal Decomposition in the Analysis of Turbulent Flows," *Annual Review of Fluid Mechanics*, Vol. 25, 1993, pp. 539-575.
[16] Cordier, L., and Bergmann, M., in *Lecture Series 2002-04 post-processing of experimental and numerical data*, (Von Karman Institute For Fluid Dynamics, 2002).
[17] Rowley, C.W., Mezic, I., Bagheri, S., Schlatter, P., and Henningson, D.S., "Spectral analysis of nonlinear flows", *J. Fluid Mech.*, Cambridge University Press 2009, pp. 1-13.
[18] Schmid, P.J., "Dynamic mode decomposition of numerical and experimental data", *J. Fluid Mech*. ,Vol. 656, 2010, pp. 5-28.
[19] Harvazinski, M.E., Anderson, W.E., and Merkle, C.L., "Combustion Instability Diagnostics Using the Rayleigh Index", *47th AIAA/ASME/SAE/ASEE Joint Propulsion Conference & Exhibit*, 31 July – 03 August 2011, San Diego, California.